Microphysical modeling of orographic cirrus clouds

Peter Spichtinger[1]*, **Andreas Dörnbrack**[2]
(1) Institute for Atmospheric Science and Climate, ETH Zurich, 8092 Zurich, Switzerland
(2) Institut für Physik der Atmosphäre, Deutsches Zentrum für Luft- und Raumfahrt, Oberpfaffenhofen, Germany

1. Introduction

One of the most challenging problems in atmospheric science is the prediction of future climate change. So far, estimates of the net radiative forcing of clouds is very uncertain. Especially, the role of cirrus clouds which could contribute to a net heating of the underlying troposphere is heavily discussed. For determining the contribution of cirrus clouds to the global warming and predicting their role in a changing climate we have to increase our knowledge on their formation processes including realistic estimates of their lifetime, their spatial spread and dispersion. Currently, observational information about the life cycles of cirrus clouds including their specific formation regions, i.e. the ice supersaturated regions, is very limited.

Additionally and as suggested by recent studies, the impact of mesoscale dynamical processes as well as the possible impact of aerosols on the life cycle of cirrus clouds is crucial for a reliable estimate of the radiative forcing. As discussed in Dean et al. (2005), exclusive consideration of synoptic-scale dynamics underestimates the frequency of occurrence of cirrus clouds. As suggested in that paper, mesoscale processes should be taken in to account, e.g. cirrus clouds generated by internal gravity waves.

From an experimental point of view, mountain-wave induced cirrus clouds constitute an ideal natural laboratory to investigate the properties and the life cycle of their cloud particles. Several experimental studies documenting these processes have been published so far. However, numerical simulation of orographic cirrus clouds are rare, especially full 2D/3D model studies. Here, first of all we focus on numerical experimentation. The goal of this study is to determine the influence of mesoscale dynamics on the generation and evolution of mountain-wave induced cirrus clouds.

Cirrus clouds formed by orographic waves are simulated with the anelastic, non-hydrostatic geophysical fluid solver EuLag. Recently, a bulk scheme for different classes of ice was developed and implemented into this model. Our microphysical scheme is able to discriminate between the different nucleation processes (homogeneously and heterogeneously formed ice crystals). For each ice class, a background aerosol number concentration was included which acts as a limiting factor for the number of nucleated ice crystals. In this way, we are able to investigate the impact of the competiting formation processes on the generation and evolution of mountain-wave induced cirrus clouds.

In section 2 we describe the model, especially the newly implemented ice microphysical scheme. In section 3 the setups for the reference experiments are described. Then, in section 4 we present first results. Finally, we summarize our results and present an outlook on future studies.

2. Description of the model

Our numerical experiments are performed with the multiscale, nonhydrostatic anelastic model EULAG (see e.g. Smolarkiewicz and Margolin 1997). An up-to-date comprehensive description of the model and its capabilities can be found in (Grabowski and Smolarkiewicz 2002) and (Prusa and Smolarkiewicz 2003). The governing

*peter.spichtinger@env.ethz.ch

equations are solved by means of finite difference approximations using a second-order accurate nonoscillatory forward-in-time approach. In the following, we discuss the bulk ice microphysics scheme.

In general, prognostic equations for both the ice water content (IWC) and the ice crystal number (N) concentration are solved with the same finite difference approximations as the equations for momentum and heat. Hence, our microphysical approach relies on a so–called double moment scheme. Here, we have to assume a mass distribution $f(m)$ for the ice crystals at each grid point, $\mu_k[m] := \int m^k f(m) dm$ denotes the kth moment of the distribution. Our ice microphysics scheme treats arbitrary many classes of ice. These classes are only discriminated by the individual formation processes, i.e. the nucleation of ice crytals. Additionally, for each formation process a background aerosol (number concentration of the background aerosol) is included which triggers the formation process directly.

In the present study, we only consider two classes, homogeneously and heterogeneously formed ice crystals. For each class of ice we prescribe a log–normal distribution as mass distribution with geometric mean mass m_m and geometric mass standard deviation σ_m. In the following, we assume columnar shape for the ice crystals with size–mass relations according to Heymsfield and Iaquinta (2000). The parameterized processes in the microphysical scheme consist of nucleation, deposition growth/evaporation and sedimentation of ice crystals.

In our scheme, two different nucleation processes are considered: First, homogeneous freezing of supercooled aqueous solution droplets and second, heterogeneous freezing on solid aerosol particles. The homogeneous nucleation rates are parameterized according to Koop et al. (2000) in terms of temperature and water activity (i.e. relative humidity). Additionally, the volume of the solution droplets (in this case aqueous sufuric acid droplets) is calculated from a prescribed size distribution of the sufuric acid aerosol and deliquescence according to Koehler's theory. For simulating the heterogeneous nucleation we start with a very simple approach: If the environmental relative humidity with respect to ice is larger than a threshold value, i. e. $RHi \geq RHi_{het}$, then all particles of the background aerosol N_a are transferred to ice crystals with an initial ice crystal mass $m_{het} = 10^{-16}$ kg. This mass is equivalent to a size of $l_{het} = 0.22\mu$m (using the size–mass relation).

For deposition growth and evaporation we use a modified approach by Koenig (1971), which was sucessfully applied in former studies (e.g. Gierens 1996): $\frac{d\mathrm{IWC}}{dt} = a \cdot \mu_b[m]$. Detailed descriptions of the individual parameterisations of nucleation and deposition in the cirrus cloud model can be found in Spichtinger et al. (submitted to ACPD).

For the sedimentation of the ice crystals we use two different terminal velocities (mass weighted and number weighted, $v_{t,m}, v_{t,n}$) derived from the flux density concept, see Gierens et al. (submitted to Quart. Jour.). In this parameterisation, larger crystals fall faster than smaller ones which should be self–evident but this is not always fulfilled in large-scale models (see extended abstract by Spichtinger et al. in this volume).

3. Description of the reference experiments

3a. *Vertically propagating hydrostatic wave*

For the generation of vertically propagating hydrostatic waves we use the following setup: we prescribe a 2D domain (x–z–plane) with a horizontal extension of 639 km and a vertical extension of 15 km. The horizontal and vertical resolutions amounts to $dx = 1$ km and $dz = 50$ m, respectively. A Gaussian hill with halfwidth $w = 15$ km and height 600 m is located at the lower bottom in the center of the domain. The simulation time amounts to 4.5 h with a dynamical time step $dt = 5$ s and an optional microphysical timestep $dtccp = dt/10 = 0.5$ s.

The model is initialized with the following vertical profiles: For the ambient potential temperature θ we prescribe a piecewise linear profile: In the range $0 \leq z \leq 12$ km the temperature gradient has the slope $d\theta/dz = 0.0025$ K/m, in the range $12 \leq z \leq 15$ km the potential temperature increases with $d\theta/dz = 0.3$ K/m, and at the tropopause ($z_{tp} = 12$ km) the transition of both is continuous. For the ambient pressure profile $p(z)$ is prescribed according to Clark and Farley (1984). From $\theta(z)$ and $p(z)$, the physical temperature $T(z)$ and the density $\rho(z)$ can be calculated.

Additionally, a horizontal wind profile $u(z)$ is prescribed: In the vertical range $0 \leq z \leq 1$ km $u(z)$ in-

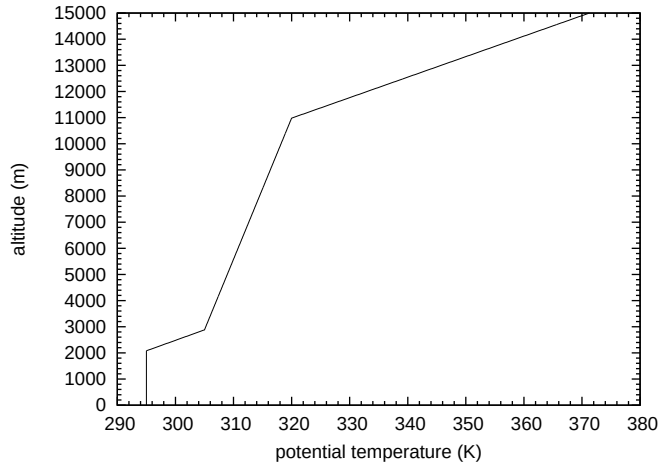

Figure 1: Vertical profile of potential temperature θ for the trapped wave case.

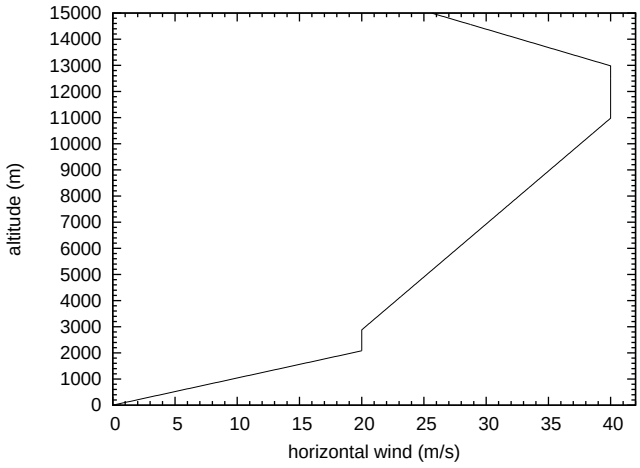

Figure 2: Vertical profile of the horizontal wind speed for the trapped wave case.

creases linearly with altitude until a value u_0 is reached. In the vertical range up to the tropopause the wind remains constant ($u(z) = u_0$), above that level, $u(z)$ decreases linearly until $u(z = 15$ km$) = -10$ m/s.

The relative humidity with respect to ice in the whole 2D domain is prescribed as $RHi = 40\%$ in the vertical range $z \leq 12$ km and $RHi = 5\%$ in the stratosphere. Additionally, a supersaturated box ($RHi = RHi_2 \geq 100\%$) in the horizontal range $60 \leq x \leq 160$ km and the vertical range $z_1 \leq z \leq z_2$ is prescribed. In this supersaturated layer we expect the cirrus cloud formation due to the adiabatic cooling in the uplift region of the mountain wave. We vary the altitude of the supersaturated layer, but the layer has always a thickness of $\Delta z = z_2 - z_1 = 1$ km. For the reference simulation we choose: $RHi_2 = 110\%$, $u_0 = 20$ m/s, $z_1 = 9.5$ km, and $z_2 = 10.5$ km, respectively.

3b. *Trapped waves*

For the simulation of trapped waves we use the same 2D domain but apply higher spatial and temporal resolutions: $dx = 500$ m, $dz = 100$ m and $dt = 2$ s. Here, the mountain with a height of 1000 m is located at 3/5 of the whole horizontal extension. The relative humidity is prescribed as in the case of the hydrostatic wave. Vertical profiles of $\theta(z)$ and $u(z)$ are prescribed as shown in Figs. 1 and 2 (see also Hertenstein and Kuettner 2005). These upstream profiles are based on rotor observations in the lee of the Sierra Nevada during the Sierra Wave Project in 1952. They allow a combined simulation of vertically propagating waves in conjunction with trapped waves in the lee. The negative vertical shear above 13 km altitude leads to stratospheric wave breaking (not discussed here). In contrast to the numerical experiments of Hertenstein and Kuettner (2005), no explicit friction was used in our simulations.

4. Results

First, we present pictures from the life cycle of the hydrostatic wave (fig 3). After approximately 90 min, the hydrostatic wave has reached the upper troposphere. In the ascending branches of the mountain wave, the background relative humidity of $RHi = 40\%$ increases up to a value of 80% due to the adiabatic cooling. The elevated supersaturated layer is advected toward the mountain wave. By passing the wave, the air parcels are lifted, RHi increases, and homogeneous nucleation takes place. The resulting ice crystals propagate downstream of the wave crest. However, the subsequent warming of the downdraft is strong enough to evaporate most of the ice crystals. Hence, only the *cirrus lenticularis* over the mountain can be simulated during the short

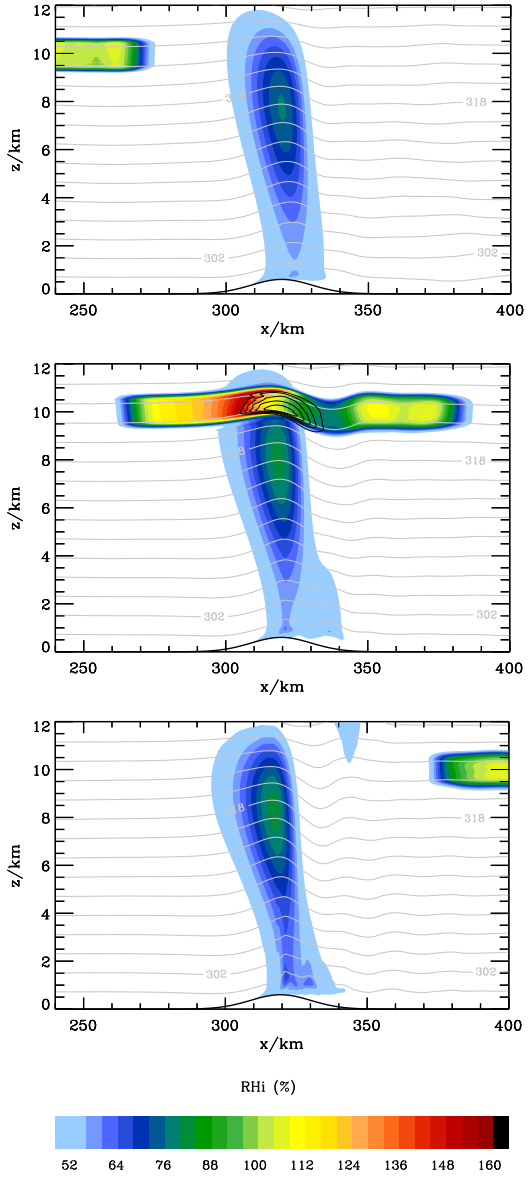

Figure 3: Relative humidity RHi (%, color shaded) and potential temperature θ (K, grey contour lines with $\Delta\theta = 2\,K$) and ice water content (mg/m^3, black contour lines with $\Delta\mathrm{IWC} = 1\,mg/m^3$) for the case of a vertically propagating hydrostatic wave at t = 90, 180, and 270 min (top, middle, bottom), respectively.

period of the passing supersaturated layer. After that time, the pre-cirrus state is reached directly above the mountain crest whereas the box itself lost its supersaturated initial state.

Figure 4 presents snapshots form the life cycle of a cirrus cloud formed above a region of trapped waves. In this case, wave energy propagates vertically as well as horizontally. After about 105 min, three crests of the trapped waves formed downstream of the mountain ridge with a typical horizontal wavelength of about 10 to 15 km. Above that region and below the tropopause, the vertically propagating hydrostatic wave generated an ascending branch where ice crystals formed during the period of the passing supersaturated box. In contrast to the vertically propagating hydrostatic mountain wave case, here, the lifted region extends horizontally downstream more than 50 km (Fig. 4b). This results in a cirrus cloud with a longer life time and a more diffusive downwind tail. Furthermore, and probably due to the steeper hill, the upstream edge of the cirrus clould is much sharper than that of the cloud shown in (fig 3b). It is interesting to note that the initially coherent supersaturated box becomes disrupted upstream of the steep displacements of isentropes above the mountain (Fig. 4b). In this way, the final picture in Fig. 4c resembles orographic cirrus clouds downstream of real mountains.

5. Summary and outlook

Using a bulk ice microphysical scheme which was recently implemented in the EULAG we were able to simulate the formation and evolution of cirrus clouds formed in the updrafts of orographic waves.

In our idealized numerical experiments we considered the formation of a cirrus cloud in a vertically propagating hydrostatic mountain wave and a mountain-wave induced cirrus cloud formed above a region of trapped waves. The life cycle of the simulated cirrus clouds depended strongly on several conditions, like the initial supersaturation ratio of the supersaturation layer, the altitude of the layer, the height and width of the hill, the horizontal velocity and the thermal stability.

For all these parameters, the sensitivities were tested and different behaviour of the simulated cirrus clouds and their lifecycles was analysed. Additionally, we

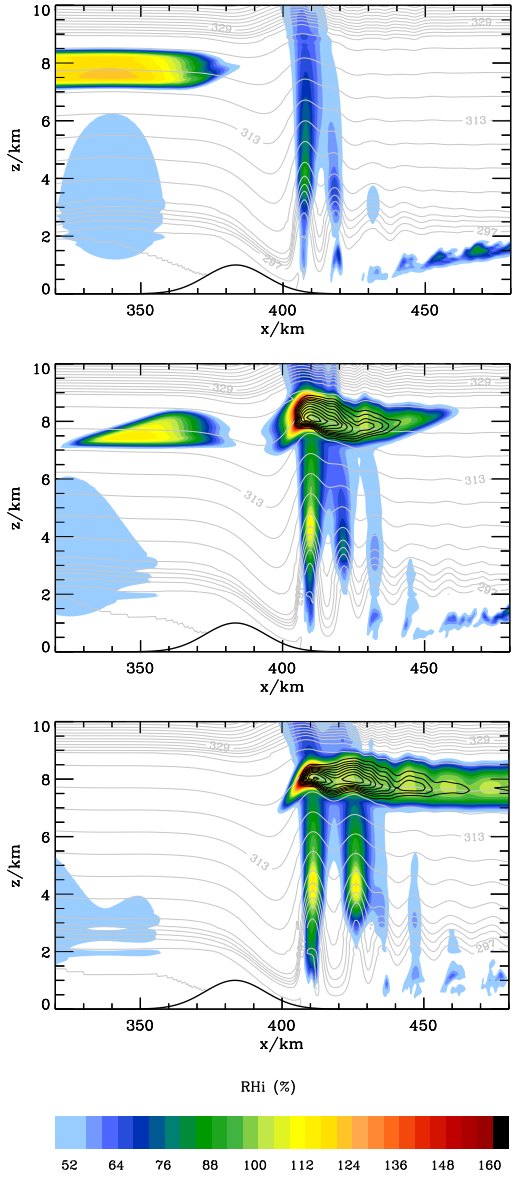

Figure 4: Relative humidity RHi (%, color shaded) and potential temperature θ (K, grey contour lines with $\Delta\theta = 2\,K$) and ice water content (mg/m^3, black contour lines with $\Delta\mathrm{IWC} = 1\ mg/m^3$) for the case of a trapped lee wave at t = 105, 135, and 185 min (top, middle, bottom), respectively.

will present numerical simulation results initialized with ECMWF data for observed cirrus clouds from the recent field campaign T-REX (Terrain-Induced Rotor Experiment, see: http://www.joss.ucar.edu/trex/).

Acknowledgement We thank Piotr K. Smolarkiewicz for sharing his model and many fruitful and exciting discussions! The numerical simulations were performed on the high performance computer facilities at the European Centre for Medium–Range Forecasts during the special project “Ice supersaturation and cirrus clouds”.

References

Clark, T. and R. Farley, 1984: Severe downslope windstorm calculations in two and three spatial dimensions using anelastic interactive grid nesting: A possible mechanism for gustiness. J. Atmos. Sci., 41, 329–350.

Dean, S., B. Lawrence, R. Grainger, D. Heuff, 2005: Orographic cloud in a GCM: the missing cirrus. Climate Dynamics 24, 771–780.

Gierens, K., 1996: Numerical simulations of persistent contrails. J. Atmos.Sci.,3333–3348.

Grabowski W. W. and P. K. Smolarkiewicz, 2002: A multiscale anelastic model for meteorological research. Mon. Weather Rev., 130, 939–956.

Heymsfield, A. and J. Iaquinta, 2000: Cirrus crystal terminal velocities. J. Atmos. Sci., 57, 916–938.

Koenig, L., 1971: Numerical modeling of ice deposition. J. Atmos. Sci., 28, 226–237.

Koop, T., B. Luo, A. Tsias, T. Peter, 2000: Water activity as the determinant for homogeneous ice nucleation in aqueous solutions. Nature 406, 611-614.

Hertenstein, R. and J. Kuettner, 2005: Rotor types associated with steep lee topography: influence of the wind profile. Tellus A 57, 117–135.

Prusa, J. M. and P. K. Smolarkiewicz, 2003: An all-scale anelastic model for geophysical flows: dynamic grid deformation. J. of Comp. Physics, 190, 601–622.

Pruppacher, H. and J. Klett, 1997: Microphysics of Clouds and Precipitation, Kluwer Acad. Pub., Dordrecht.

Smolarkiewicz, P. and Margolin, L., 1997: On forward–in–time differencing for fluids: an Eulerian/Semi–Lagrangian non–hydrostatic model for stratified flows. Atmosphere–Oceans, 35, 127–152.

Smolarkiewicz, P., L. Margolin, A. Wyszogrodzki , 2001: A class of nonhydrostatic global models. J. Atmos. Sci., 58, 349–364.